HHS Public Access

Author manuscript

Chem Commun (Camb). Author manuscript; available in PMC 2019 May 31.

Published in final edited form as:

Chem Commun (Camb). 2018 May 31; 54(45): 5700–5703. doi:10.1039/c8cc01263f.

The distinct structural preferences of Tau protein repeat domains

Xuhua Li[a], **Xuewei Dong**[a], **Guanghong Wei**[a,*], **Martin Margittai**[b], **Ruth Nussinov**[c,d,*], and **Buyong Ma**[d]

[a]Department of Physics, State Key Laboratory of Surface physics, Key Laboratory for Computational Physical Science (Ministry of Education), Collaborative Innovation Center of Advanced Microstructures (Nanjing), Fudan University, Shanghai 200433, People's Republic of China

[b]Department of Chemistry and Biochemistry, University of Denver, Denver, CO 80208

[c]Sackler Inst. of Molecular Medicine Department of Human Genetics and Molecular Medicine Sackler School of Medicine, Tel Aviv University, Tel Aviv 69978, Israel

[d]Basic Science Program, Leidos Biomedical Research, Inc. Cancer and Inflammation Program, National Cancer Institute, Frederick, MD 21702, USA

Abstract

The tau fibrillar structures from the brain of an Alzheimer's patient have a core with C-shaped motif of third and fourth repeat domains (R3-R4). Our simulations indicated that the C-shaped motif is only stable for the R3-R4, while R1-R2 tends to be linear in shape. These two structural motifs appear in the most stable K18 protofilament. Heparin can further stabilize the C-shaped R3-R4 motif, but not other repeats.

TOC image

Among the four bi-repeat protofilaments, only R3-R4 can maintain C-shaped structure that can be stabilized by heparins, while R1-R2 tends to be linear shape, and these two structural motifs appear in the most stable K18 protofilament.

* nussinor@mail.nih.gov; ghwei@fudan.edu.cn.

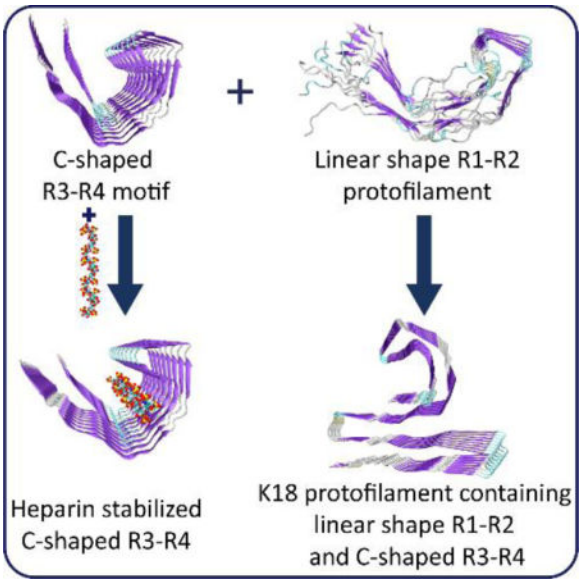

One of the hallmarks of Alzheimer disease is amyloid deposit formed by amyloid-β (Aβ) plaques and tau protein tangles.[1] Aβ plaques enhance Alzheimer's brain tau-seeded pathologies by facilitating tau aggregation,[2] possibly through a "stretching-and-packing" cross-seeding mechanism.[3] Both Aβ and tau can trigger neuroinflammation and lead to neuro-degeneration.[4] Interest is growing in tau as a potential drug target, by blocking tau aggregation.[5] Two major types of isoforms exist for tau proteins, with either three (R1, R3 and R4) or four (R1~R4) microtubule binding repeats (MBR). K18 is one of the truncated constructs of tau, consisting of four repeats. During tau aggregation, the MBR domain becomes structured and forms a protease-resistant core. Studies of tau amyloids are complicated because of potential structural differences between filaments in different tau-related diseases[6]. Structural variations in tau filaments have also been observed *in vitro* and could be further modulated by polyanionic amyloid inducers such as heparin.[7, 8] Previous molecular dynamic (MD) simulations and EPR experiments reported linear straight or β-turn-β U-shaped motifs for the four repeats.[9–12] An electron microscopy study showed that tau filament cores consist of a double helical stack of C-shaped subunits.[13] Recently, the atomic details of repeats R3-R4 plus 10 ten extra C-terminal residues (residues 306~378) of filament cores were revealed by high resolution Cyro-EM[14], provided important insights into the polymorphic tau protein tangles. However, whether other bi-repeat combinations R1-R2, R1-R3 and R2-R3 have a preference to adopt a C-shaped structure remains elusive. Since in AD all isoforms are incorporated into amyloid core, the structural compatibility of different repeats is one of keys to understand prion-like properties of tau protein aggregation.

Here we examine the stabilities of the octameric C-shaped structural motifs (Fig. S1A ESI†) formed by different bi-repeat combinations with or without heparins and different conformations of K18 protofilaments. All-atom explicit-solvent MD simulations were performed for twenty-four various tau protofilaments and filaments (see Methods ESI†).

†Electronic Supplementary Information (ESI) available: 3 Tables and 10 figures.

We first examined the stabilities of all possible bi-repeat (Fig. 1A and Fig. S1B-C ESI†) C-shaped motifs (R1-R2 (residues 244~315), R2-R3 (residues 275~346), R1-R3 (residues 244~274 and 306~346), and R3-R4 (residues 306~378)) in both paired helical filaments (PHFs) and straight filaments (SFs). According to the recent Cryo-EM work, a filament consists of two protofilaments.[14] The protofilament system includes five different bi-repeat combinations: PHF_{34}, PHF_{12}, PHF_{13}, PHF_{23} and SF_{34} (Fig. 1A and Fig. S1B). The filament system includes four different PHF and SF filaments: $2PHF_{34}$, $2PHF_{12}$, $2PHF_{13}$, $2PHF_{23}$, $2SF_{34}$, $2SF_{12}$, $2SF_{13}$, and $2SF_{23}$ (Fig. 1A and Fig. S1C ESI†). The structures of R3-R4 protofilaments and filaments were taken from cryo-EM coordinates, and other combinations were constructed using the R3-R4 structures as templates.

The stability of all PHF protofilaments are examined by probing the trajectories of RMSD and hydrogen bond (H-bond) number, and the RMSF (Fig. 1B-D). The RMSD shows that PHF_{34} structure stabilizes quickly around 0.30 nm, while PHF_{12}, PHF_{13} and PHF_{23} continue to deviate from their initial structures, with their RMSDs reaching to respectively, 0.93 nm, 0.95 nm and 0.83 nm at t= 100 ns (Fig. 1B). Consistently, H-bond number of PHF_{34} fluctuates around 480, while that of other three protofilaments decreased rapidly (Fig. 1C). The RMSF values show that almost all β regions (Fig. S1B ESI†) in PHF_{34} exhibit the highest rigidity (Fig. 1D). The high structural stability of PHF_{34} can also be seen from the residue-based β-sheet probability (Fig. S2A ESI†). We characterize the C-shaped structure by monitoring the β2-β3/β6-β7 angles and a distance between two representative residues in β6 and β8 (i.e. Q_{351}-I_{371} in PHF_{34}, Q_{288}-I_{308} in PHF_{12}, and T_{319}-V_{339} in PHF_{13} and PHF_{23}) (Fig. 1E-G). The β2-β3 and β6-β7 angles in PHF_{34} stay respectively around 100° and 73° throughout simulations. But the β6-β7 angles in PHF_{13} and PHF_{23} increase to 116° and 118° at t=100 ns, implying that structures in β6 and β7 regions of PHF_{13} and PHF_{23} tend to be extended. In PHF_{12}, though the β6-β7 angle (75°) stays close to that in PHF_{34}, the β2-β3 angle is much larger than 100°, indicating that PHF_{12} has a strong tendency to be straight (Fig. 1H). The β-sheet distance confirmed the instability of the C-shaped PHF_{12}, PHF_{13} and PHF_{23}. Although the value of the β2-β3 angle in PHF_{34}, PHF_{13}, and in PHF_{23} at t=100 ns are same, the distance between β6 and β8 in PHF_{13} and PHF_{23} is much larger than that in PHF_{34} system. The distance increase in the former two systems is mainly caused by the twisting of β1-β2 plane relative to β3 plane (Fig. S2C ESI†). PHF_{23} is prone to be V-shaped, and PHF_{13} has a preference to be U-shaped, as seen from the final snapshot (Fig. S2C ESI†). These results indicate that PHF_{34} can maintain its C-shaped structure well, while the other three are not compatible with the C-shape structure. Similar structural stability is observed for SF_{34}. (Fig. S3 ESI†) Note that β8 is not in tau repeats domain but have a large interface with β1~β2, and it helps the shape formation of the four in the order of PHF_{12} > PHF_{34} > PHF_{13} > PHF_{23} (Supplementary Materials).

To understand why the other three protofilaments cannot be stabilized in a C-shaped structure, we examine the inter-chain and intra-chain pairwise residue contact probability (Fig. S4 ESI†). The contact pattern of PHF_{34} reflects that the interactions between the C-terminal residues of one chain and the N-terminal residues of the nearby chain helps to stabilize the C-shaped structure (Fig. S4A ESI†). Other three bi-repeat protofilaments have weak interactions. In the PHF_{12}, the interactions in β1, β3, β7 and the β8 C-terminal regions are reduced. In the PHF_{13}, the regions with weakened interactions change to β1, β3, β5 and

β7. In PHF_{23}, β3, β5 and β7 are the weak interaction regions. Intra-chain interactions are also important in maintaining the C-shaped structure. PHF_{34} has the strongest intra-chain interactions (Fig. S4B ESI†). In the PHF_{34}, the interactions among K_{353}, S_{356} and D_{358} residues stabilize the β6-β7 angle and the interactions among C_{322}, L_{325}, I_{328}, P_{364} and G_{367} can stabilize the β2-β3 angle (Fig. S4C ESI†), while in other systems, the two angles cannot be simultaneously stabilized around their initial values. The lack of intra-chain interactions between P_{301} and G_{304} explains the extension of PHF_{12} (Fig. S4B and Fig.1H). The β6-β7 angle is stabilized by the salt-bridges K_{353}/D_{358} in PHF_{34} and K_{290}/D_{295} in PHF_{12} (Fig. S4D ESI†). However, these two salt-bridges are missing in the other two systems. The destabilization of the C-shaped structure of PHF_{13} and PHF_{23} can be seen in Fig. S2C.

The structural differences between MBR have a great effect on interaction patterns among the four protofilaments (Fig. S5 ESI†). In the PHF_{34} system, the hydrophobic residues of the hexapeptide V_{306}~K_{311} in β1 and T_{373}~F_{378} in β8 form a face-to-face packing interface. However, similar interactions in both PHF_{12} and PHF_{13} were missing due to the reduced number of hydrophobic residues in β1. In addition, three consecutive β-breaking prolines (P_{247}, P_{249}, and P_{251}) destroy the β-sheet structure of β1 and the N-terminal region of β2, and the β-sheet structure of C-terminal regions of β8 in PHF_{12} is also disrupted by P_{312}. In PHF_{34}, there is a right-angle turn accomplished through G_{323} and G_{326} on the outer side of the C-shaped protofilament, while in the other three systems, the reduced number of Glycine is not sufficient for keeping the turn of the C-shaped structure. In the PHF_{34} system, a triangle-shaped hydrophobic cluster formed by L_{325} in the turn region, I_{328} in β3 and V_{363} in β7. However, in PHF_{12}, the cluster disappears and lead to an extended turn conformation. In the PHF_{13} and PHF_{23} systems, there is only one hydrophobic residue in the hydrophobic cluster region, which greatly reduces the stability of that region. The β4~β6 regions in PHF_{34} system form a β-helix structure. Two-residue (E_{342} and K_{343}) and three-residue (K_{347}, D_{348} and R_{349}) β-arc corners facilitate the triangular β-helix geometry, whereas, residues in the corresponding β-arc position are not favorable for β-arc formation. In addition, hydrophobic (V_{339}, L_{344}, V_{350}, and I_{354}) and aromatic (F_{346}) residues stabilize the interior of the β-helix geometry in PHF_{34}. However, aromatic residues are missing in all the other systems. Moreover, the β-breaking residue P_{312} in PHF_{34} is located between β1 and β2, while proline residues are missing at the corresponding position in PHF_{23}, which renders the β1 and β2 to combine into a longer β-strand. And this makes the whole structure of PHF_{23} look like a V shape. (Fig. S2 ESI†).

The dimerization of protofilaments cannot help stabilizing other repeat combinations in the C-shaped structure, but is favourable for R3-R4, indicated by MD simulations of octameric 2PHF and 2SF filaments (a tetramer for each protofilament) in four bi-repeat combinations. (Fig. S6B ESI†) In cryoEM-derived $2PHF_{34}$, the interface is formed by the anti-parallel stacking of residues P_{332}~Q_{336}. The corresponding residues in the interface are P_{270}~K_{274} for both PHF_{12} and PHF_{13}, and P_{301}~S_{305} for PHF_{23}. Fig. S7A shows the contact probabilities of eight interface residues of all 2PHF combinations. Overall, the protofilament interfaces of $2PHF_{34}$ and $2PHF_{23}$ are more stable than those of $2PHF_{12}$ and $2PHF_{13}$. In the $2PHF_{12}$ and $2PHF_{13}$, the interface interactions are weak and the two protofilaments tend to separate (Fig. S7B ESI†). Both protofilaments in the $2PHF_{34}$ system retain the C-shaped structure well, while all others have conformational deviations from the C-shaped structure.

In cryoEM-derived $2SF_{34}$, the two protofilaments pack asymmetrically between residues K_{321}~S_{324} in one protofilament and V_{313}~K_{317} in the other. To compare with 2PHF, we also choose eight residues in each protofilament (K_{317}~S_{324} and D_{314}~K_{321}) to analyze the interface stability. The contact probability maps and the last frame snapshots in Fig. S7 and Fig. S8 show that compared to $2PHF_{34}$, $2SF_{34}$ has weak interface interactions involving residue pairs L_{315}-K_{321} L_{315}-C_{322} and L_{315}-G_{323}. In the SF_{34} protofilament interface, consistent with Cryo-EM, the main interactions are strong VdW interactions between L_{315}-K_{321} L_{315}-C_{322} and L_{315}-G_{323} (Fig. S8A ESI†). In the $2SF_{12}$ system, the two protofilaments separate. The interface contact residues in $2SF_{13}$ and $2SF_{23}$ are respectively L_{253}-K_{259}, L_{253}-I_{260}, L_{253}-G_{261} and N_{255}-K_{259}, and L_{284}-K_{290}, L_{284}-C_{291}, L_{284}-G_{292} and N_{286}-K_{290}, like those in $2SF_{34}$. (Fig. S8A ESI†) More results and discussion the contributions of dimerization to the shape formation be found in Supplementary Materials.

Full-length tau quickly aggregates when anionic cofactors are present.[15] In in vitro experiments, heparin is often used to induce and accelerate tau filament formation.[16–18] In vivo, it has been reported that tau and heparin coexist in neurons with overt neurofibrillary lesion.[19] However, how heparin promotes tau fibrillation is unclear. Also, whether it is a component of tau filaments is open to debate.[20, 21] The C-shaped structural feature of tau filaments suggests that heparin could fit into the groove of the protofilament to stabilize its structure (Fig. 2). The length of hexameric heparin is comparable to the length of the groove of octameric PHF protofilaments. Thus, we simulated the tau protofilament-heparin complex (PHF-HP) to examine if heparin can stabilize the C-shaped core.

Fig. 2 indicates that, among all PHF-HP systems simulated, PHF_{34}-HP is the most stable one. Even though heparin reduces structural flexibilities of all bi-repeat combinations, only PHF_{34}-HP system maintains its C-shaped structure (Fig. S9A ESI†). Even though the RMSD of PHF_{13} decreases from 0.90 nm to 0.71 nm, it is still not comparable to the 20.7% reduction in RMSD from 0.29 nm to 0.23 nm observed for the protofilament in the PHF_{34}-HP system (Table S2). The RMSFs reflect an increased flexibility of other systems, compared to that in the PHF_{34}-HP system (Table S3). Heparin reduces the flexibility of most regions in the protofilaments. In the PHF_{34}-HP system, in addition to the slightly decreased rigidity of β3, the rigidity of the overall structure is enhanced. However, for other protofilaments, there is only localized enhancement of rigidity. PHF_{34} has the highest probability of β-sheet, followed by PHF_{23}, PHF_{13} and PHF_{12}. These results show that the repeats R3-R4 are most suited to interact with heparin and accelerate tau fibrillization.

Why is heparin able to selectively stabilize R3-R4 to adopt a C-shaped structure? We examine the contact probability between heparin and each protofilament by excluding the edge strands (Fig. S9 ESI†). In the PHF_{34}-HP system, there are three regions involving seven residues (R_{349}, Q_{351}, K_{353}, I_{360}, H_{362} K_{369}, and I_{371}) that have strong contacts with heparin. Positively charged K_{353} and K_{369} attractively interact with polyanion heparins. Q_{351} also displays high contact probability with heparin. Residues I_{371} and Q_{351} are likely to serve as a gate to keep heparin inside the groove. The attraction between R_{249} and heparin also helps stabilizing the C-shaped structure. Other three systems only have two or three residues strongly interacting with heparin, which can maintain the local but not global structures. In the PHF_{12}-HP system, K_{290} and H_{299} have high contact probabilities with

heparin. However, RMSF values revealed that although the strong interaction between K_{290} and heparin can stabilize the β4~β6 regions, the interaction between H_{299} and heparin destabilizes the β3 and β7 (Table S3). Similarly, fewer basic residues in other repeat systems (K_{321} in PHF_{13} and PHF_{23}) do not provide sufficient interactions to stabilize the C-shaped structure.

Previous experiments[22, 23] reported that the core of tau filaments is formed by three or four repeats. Only bi-repeat constructs were considered in above-mentioned simulations. When all four repeats are considered (such as in K18) two questions arise: 1) Can R1-R2 also be stabilized in C-shape? 2) Is the C-shaped R3-R4 motif compatible with a different shape of the R1-R2 motif? To answer these questions, we simulate K18 with the C-shaped R3-R4 in combination with different shapes of R1-R2 motif. We termed them K18-1, -2, -3, -4, -5, -6, and -7. All the initial structures are shown in Fig. 3A.

Figure 3 shows that, K18-2, where R1-R2 is in linear and R3-R4 is in C-shape, has the lowest energy and the smallest RMSD, followed by K18-5 (with a linear shaped R1-R2) and K18-3 (with a compact U-shaped R1-R2). K18-1, the structure with two C-shaped motifs, has small RMSD, but high energy. (Fig. 3C) By comparing the GBMV energies with those in our previous work,[12] we found that the energies of all K18 structures containing the C-shaped R3-R4 motif are respectively lower than those of conformers with the same R1-R2 conformations. Interestingly, we found that in K18-2, 16 residues (i.e. K_{290} to S_{305}) in R2 are well packed with R3. The cryo-EM indicated that residues from R1 or R2 may form an additional, less-ordered β-sheet.[14] The relative position between these 16 residues and the C-shaped R3-R4 resembles that in the cryo-EM electron density map of tau filament cores.[14] While residues from the N-terminal region may also contribute to the observed cryo-EM, our simulation indicated that the stability of C-shaped of R3-R4 does not depend on the structurally unsolved region. Overall, our data indicate that the K18 protofilament is most likely to adopt the K18-2 conformation (Fig. 3D).

In summary, our data indicate that only the R3-R4 motif can maintain the C-shaped structure, while R1-R2 tends to be linear. The high β-sheet probability and stable interface of R2-R3 suggest that R2-R3 might also be a good candidate. However, whether it can exist in C-shape remains to be seen. Heparin may stabilize the C-shaped R3-R4 motif. Notably, the interactions in other repeat combinations are not strong enough to stabilize them in the C-shaped β-sheet motif. Simulations of K18 with the C-shaped R3-R4 in combination with different shapes of R1-R2 demonstrate that the C-shaped R3-R4 motif is compatible with either a linear or compact U-shaped R1-R2 motif. The constructed K18 with a linear R1-R2 and C-shaped R3-R4 is the most stable one among all K18 conformations, indicating it's most possible to be the tau filament core. In the future, it will be interesting to see how the N- and C-terminal flanking regions in tau might affect structural stability and if the C-shaped motif is sensitive to mutations and posttranslational modifications.

Supplementary Material

Refer to Web version on PubMed Central for supplementary material.

Acknowledgments

This work was supported by NIH contract HHSN261200800001E and by the Intramural Research Program of the CCR, NCI, NIH. G. W thanks the NSF of China (Grant No. 11674065) and the National Key R&D Program of China (Grant No. 2016YFA0501702). MD simulations were performed at the Biowulf cluster at the NIH and National High-Performance Computing Center of Fudan University. We thank Dr. Scheres for providing the cryo-EM structures.

Notes and References

1. Polanco JC, Li C, Bodea LG, Martinez-Marmol R, Meunier FA, Gotz J. Nat Rev Neurol. 2018; 14:22–39. [PubMed: 29242522]
2. He Z, Guo JL, McBride JD, Narasimhan S, Kim H, Changolkar L, Zhang B, Gathagan RJ, Yue C, Dengler C, Stieber A, Nitla M, Coulter DA, Abel T, Brunden KR, Trojanowski JQ, Lee VM. Nat Med. 2018; 24:29–38. [PubMed: 29200205]
3. Qi R, Luo Y, Wei G, Nussinov R, Ma B. The Journal of Physical Chemistry Letters. 2015; 6:3276–3282.
4. Bolos M, Perea JR, Avila J. Biomol Concepts. 2017; 8:37–43. [PubMed: 28231054]
5. Li C, Gotz J. Nat Rev Drug Discov. 2017; 16:863–883. [PubMed: 28983098]
6. Crowther RA, Goedert M. J Struct Biol. 2000; 130:271–279. [PubMed: 10940231]
7. Jangholi A, Ashrafi-Kooshk MR, Arab SS, Riazi G, Mokhtari F, Poorebrahim M, Mahdiuni H, Kurganov BI, Moosavi-Movahedi AA, Khodarahmi R. Arch Biochem Biophys. 2016; 609:1–19. [PubMed: 27638048]
8. Luo Y, Yu X, Dinkel P, Zheng J, Margittai M, Nussinov R, Wei G, Ma B. Chemical Communications. 2013; 49:3582–3584. [PubMed: 23527380]
9. Adamcik J, Sanchez-Ferrer A, Ait-Bouziad N, Reynolds NP, Lashuel HA, Mezzenga R. Angew Chem Int Ed Engl. 2016; 55:618–622. [PubMed: 26636567]
10. Miller Y, Ma B, Nussinov R. Biochemistry. 2011; 50:5172–5181. [PubMed: 21506544]
11. Siddiqua A, Luo Y, Meyer V, Swanson MA, Yu X, Wei G, Zheng J, Eaton GR, Ma B, Nussinov R, Eaton SS, Margittai M. Journal of the American Chemical Society. 2012; 134:10271–10278. [PubMed: 22656332]
12. Yu X, Luo Y, Dinkel P, Zheng J, Wei G, Margittai M, Nussinov R, Ma B. The Journal of biological chemistry. 2012; 287:14950–14959. [PubMed: 22393063]
13. Crowther RA. Proceedings of the National Academy of Sciences of the United States of America. 1991; 88:2288–2292. [PubMed: 1706519]
14. Fitzpatrick AWP, Falcon B, He S, Murzin AG, Murshudov G, Garringer HJ, Crowther RA, Ghetti B, Goedert M, Scheres SHW. Nature. 2017; 547:185–190. [PubMed: 28678775]
15. Buée L, Bussière T, Buée-Scherrer V, Delacourte A, Hof PR. Brain Research Brain Research Reviews. 2000; 33:95–130. [PubMed: 10967355]
16. Pérez M, Valpuesta JM, Medina M, Montejo DGE, Avila J. Journal of Neurochemistry. 1996; 67:1183–1190. [PubMed: 8752125]
17. Taniguchi S, Suzuki N, Masuda M, Hisanaga S, Iwatsubo T, Goedert M, Hasegawa M. Journal of Biological Chemistry. 2005; 280:7614. [PubMed: 15611092]
18. Zhao J, Huvent I, Lippens G, Eliezer D, Zhang A, Li Q, Tessier P, Linhardt RJ, Zhang F, Wang C. Biophysical Journal. 2017; 112:921. [PubMed: 28297651]
19. Perry G, Siedlak SL, Richey P, Kawai M, Cras P, Kalaria RN, Galloway PG, Scardina JM, Cordell B, Greenberg BD. Journal of Neuroscience. 1991; 11:3679–3683. [PubMed: 1941102]
20. Nathalie, Sibille, Alain, Sillen, Arnaud, Leroy§, Jeanmichel, Wieruszeski, Barbara Mulloy, A. Isabelle Landrieu and Guy Lippens. Biochemistry. 2006; 45:12560. [PubMed: 17029411]
21. Carlson SW, Branden M, Voss K, Sun Q, Rankin CA, Gamblin TC. Biochemistry. 2007; 46:8838–8849. [PubMed: 17608454]
22. von Bergen M, Barghorn S, Muller SA, Pickhardt M, Biernat J, Mandelkow EM, Davies P, Aebi U, Mandelkow E. Biochemistry. 2006; 45:6446–6457. [PubMed: 16700555]

23. Wischik CM, Novak M, Edwards PC, Klug A, Tichelaar W, Crowther RA. Proceedings of the National Academy of Sciences of the United States of America. 1988; 85:4884–4888. [PubMed: 2455299]

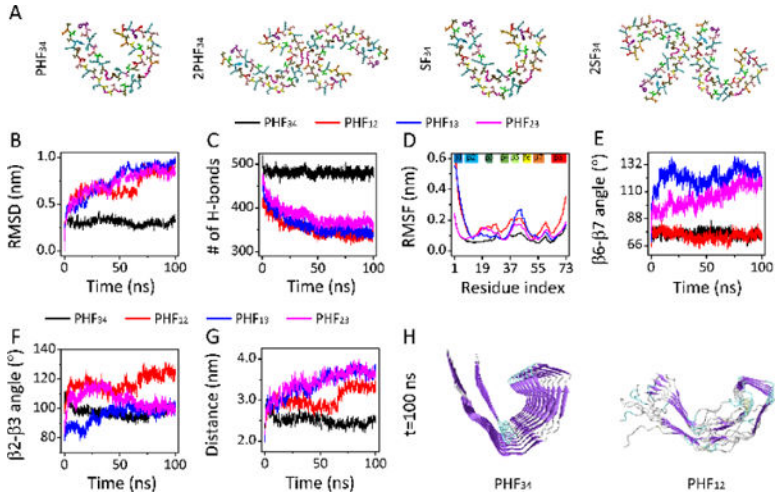

Figure 1.

Only R3-R4 PHF/SF protofilaments and filaments can maintain C-shaped structure. (A) Initial structure of a single chain in protofilaments and of two chains in filaments for the R3-R4 combination. The trajectories of the RMSD (B) and number of hydrogen bond (H-bond) (C) for four PHF protofilaments. (D) The RMSF of four PHF protofilaments. Time evolution of β6-β7 angle (E) and β2-β3 angle (F) for all protofilaments, and Q_{351}-I_{371} distance in PHF_{34}, Q_{288}-I_{308} distance in PHF_{12}, and T_{319}-V_{339} distance in PHF_{13} and PHF_{23} (G). (H) The snapshots of PFH_{34} and PHF_{12} at t=100 ns.

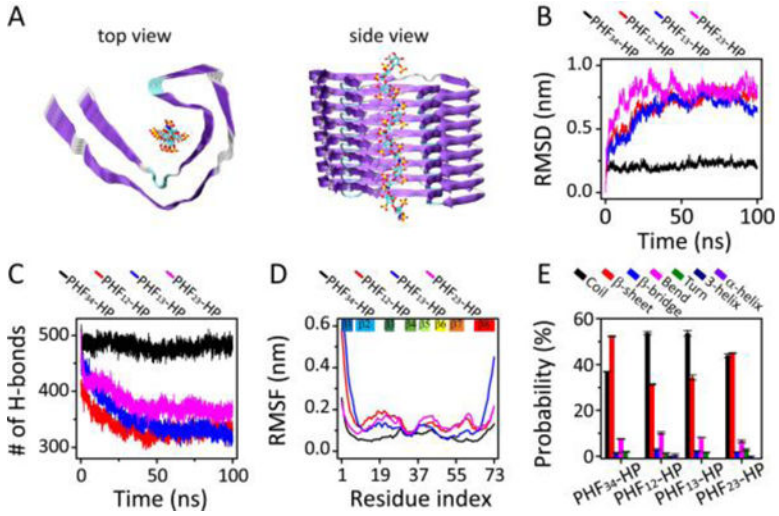

Figure 2.

The stabilization effect of heparin on four PHF combinations. (A) Initial structures of PHF-HP protofilament with side view on the left and main view on the right. Trajectories of (B) RMSD and (C) hydrogen bond number of protofilaments. (D) The RMSF of PHF-HP combinations. (E) The probabilities of each type of secondary structures.

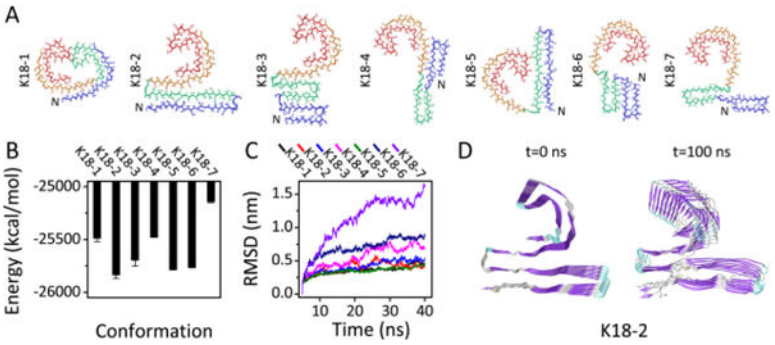

Figure 3.

Seven constructed octameric K18 protofilaments and their Stabilities. (A) The initial structures. For clarity, only one chain in each octamer is presented with R1 in blue, R2 in green, R3 in orange and R4 in red (B) The GBMV energy of each protofilament. (C) The RMSD trajectories of each protofilament. (D) Cartoon representations of initial and final snapshots of the most stable structure of K18: K18-2.